ACS APPLIED MATERIALS & INTERFACES

RESEARCH ARTICLE

www.acsami.org

# Atomic Layer Deposition of $Al_2O_3$ and ZnO at Atmospheric Pressure in a Flow Tube Reactor

Jesse. S. Jur*,† and Gregory N. Parsons‡

†Department of Textile Engineering, Chemistry and Science, North Carolina State University, Raleigh, North Carolina 27695, United States

‡Department of Chemical and Biomolecular Engineering, North Carolina State University, Raleigh, North Carolina 27695, United States

**ABSTRACT:** Improving nanoscale thin film deposition techniques such as atomic layer deposition (ALD) to permit operation at ambient pressure is important for high-throughput roll-to-roll processing of emerging flexible substrates, including polymer sheets and textiles. We present and investigate a novel reactor design for inorganic materials growth by ALD at atmospheric pressure. The reactor uses a custom "pressure boost" approach for delivery of low vapor pressure ALD precursors that controls precursor dose independent of reactor pressure. Analysis of continuum gas flow in the reactor shows key relations among reactor pressure, inert gas flow rate, and species diffusion that define conditions needed to efficiently remove product and adsorbed reactive species from the substrate surface during the inert gas purge cycle. Experimental results, including in situ quartz crystal microbalance (QCM) characterization and film thickness measurements for deposition of ZnO and $Al_2O_3$ are presented and analyzed as a function of pressure and gas flow rates at 100 °C. At atmospheric pressure and high gas flow, ZnO deposition can proceed at the same mass uptake and growth rate as observed during more typical low pressure ALD. However, under the same high pressure and flow conditions the mass uptake and growth rate for $Al_2O_3$ is a factor of ~1.5−2 larger than at low pressure. Under these conditions, $Al_2O_3$ growth at atmospheric pressure in a "flow-through" geometry on complex high surface area textile materials is sufficiently uniform to yield functional uniform coatings.

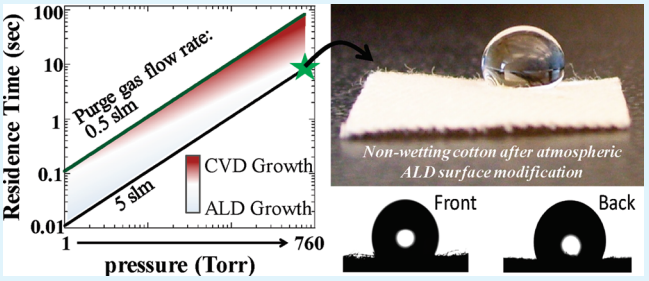


**KEYWORDS:** atmospheric pressure, atomic layer deposition, roll-to-roll, textiles, thin film growth, $Al_2O_3$, ZnO

## I. INTRODUCTION

Deposition and surface coating technologies are useful in electronics, health and biotechnology products, energy generation and storage, catalysis, optical devices, and many other systems. Over the past several years, atomic layer deposition (ALD) has emerged as an attractive thin film coating method because it achieves extremely high conformality with precise thickness control at the nanoscale to the microscale. A wide range of oxide, nitride, and elemental materials can be deposited by ALD,[1−3] and related processes for organic thin film formation are emerging.[1,4] Atomic layer deposition is particularly attractive because several materials can be grown at low operating temperatures, even as low as room temperature, allowing ALD materials to be integrated into low thermal budget processes, including electronics passivation, and coating of thermally sensitive polymers and biologically derived materials.[5−7] Even with these distinct advantages, processing constraints still impart significant restrictions on ALD. For example, the overall growth rate in ALD processes is typically much slower than in conventional chemical vapor deposition or physical deposition methods. However, batch sample processes and optimized equipment design can enable very high throughput, especially for the growing number of applications where only very thin films are needed. Another common process issue for ALD is that it typically operates at pressures of a few Torr. At typical flow rates, ~1 Torr is high enough to permit viscous flow conditions (i.e., outside the high vacuum Knudsen flow regime) so that pulses of different gas vapors can flow through the reactor without significant mixing. This helps achieve reasonable overall deposition rates by minimizing the purge time needed to physically isolate the reactant gases in the flow stream. A pressure of 1 Torr is also low enough to achieve the desired balance between advective and diffusive vapor transport. Advective transport is achieved by pumping, for example, whereas diffusive transport results from a concentration gradient. Convective transport generally refers to the combination of advective and diffusive flow. For a fixed time period, the distance a species moves by diffusion scales inversely with pressure. Fast diffusion at low pressure allows product species created on the growth surface to be quickly integrated into the flow stream and removed from the reactor, permitting relatively short gas pulse cycle times. At higher pressures where diffusivity is reduced, higher gas flow velocity can help avoid gas mixing. Analysis of diffusive and convective

Received: September 30, 2010
Accepted: January 5, 2011
Published: January 25, 2011





dx.doi.org/10.1021/am100940g | ACS Appl. Mater. Interfaces 2011, 3, 299–308

transport parameters as a function of flow rate and pressure provides helpful insight into ALD reaction process design.

Although the batch process mode for ALD is sufficient and often attractive, expanding ALD to a continuous mode process operating under ambient pressure conditions could open significant new application fields. For example, roll-to-roll ALD could be used to coat polymer sheets for packaging applications.[8−10] Recent studies show that ALD can produce uniform and conformal coatings on complex synthetic and natural fiber matrices, and the coating can change the surface wetting and functionality.[6] Modified nonwovens and textiles could provide new applications in filtration and chemical separations, protective clothing, and other areas.[11,12] A continuous ALD process operating at or near ambient atmospheric pressure could simplify functional integration of ALD materials for packaging, textiles, and other emerging applications.

Some of the earliest work on ALD reactors explored designs that were compatible with atmospheric pressure operation,[13] and since then several studies have described atmospheric pressure ALD film growth.[14−23] Precursor delivery typically involves flowing an inert gas near atmosphere pressure either over a heated solid source (e.g., Zn) or by bubbling the high pressure gas through a liquid precursor. By delivering the precursor and coreactants at physically separate sites, ALD can proceed by passing the substrate back and forth between the delivery zones. This "spatial ALD" approach allows the number of ALD cycles, and hence deposited film thickness, to be determined by the number of passes the substrate makes between the reactant introduction sites. Several studies have explored this method, for example, to deposit GaAs,[14] ZnS,[16] ZnO,[17−19] ZnO(N),[15] $HfO_2$,[20,21] and $ZrO_2$.[22,23] In one specific example, Yoshii et al.[23] deposited $ZrO_2$ films at atmospheric pressure in a flow tube system, where three flow zones were defined (containing $ZrCl_4$ vapor, $O_2$ and inert gas, respectively), and the substrate was shuttled among the zones to achieve ALD. An alternate method designed by Levy et al.[19] had the precursor, reactant, and purge gas delivered through a modified printer head with sequential A/B/C/B ports (A−precursor, B−inert gas, C−reactant). Again, ALD was achieved by moving the substrate back and forth through the precursor/reactant delivery zones. They showed that this process could readily produce stable low temperature ZnO thin film transistor devices.[19]

There are many outstanding challenges that must be addressed to achieve well-defined atmospheric pressure ALD (AP-ALD) processing. One challenge is that the precursors must be effectively delivered to a system operating at a pressure above the vapor pressure of the precursor. Second, we need to better understand how the system design parameters such as reactor geometry, gas flow rates, reactant and purge gas cycle times, and process pressures affect convective and diffusive species transport. Third, possible affects of system pressure on ALD surface reaction processes need to be understood and described. In general, reports to date on AP-ALD do not include detailed studies of process surface reactions, and how reactions are affected by the process pressure. Levy et. al[19] report that ZnO ALD at 1 atm on planar substrates produces the same thickness per cycle as a typical 1−2 Torr process. However, in situ analysis of growth mechanisms at 1 atm have not been reported. Furthermore, previous studies of high pressure ALD have not addressed the issue of film conformality on nonplanar substrates, which is a critical characteristic for many ALD applications.

In this work, we describe a unique atmospheric pressure ALD reactor system designed in a flow tube geometry, where physical movement of deposition substrate or the precursor delivery inlet is not required. Moreover, a new precursor delivery scheme allows the process pressure to be adjusted independently and fixed at values between ∼2 and 760 Torr. Using simple gas kinetic models, we evaluate mass transport parameters including Reynolds and Péclet numbers, gas residence time, and species diffusion velocity as a function of pressure and gas flow rates. Calculated parameters are then related to measured film growth rates and results from in situ quartz crystal microbalance. Initial work described here addresses ZnO and $Al_2O_3$ ALD processes. We also use our AP-ALD approach to coat high surface area fibrous substrates and demonstrate that the resulting changes in surface wetting and functionalization are similar to those obtained under more conventional ALD process conditions.[6] We expect these results to provide important system design parameters to understand the operation of AP-ALD processes for a range of advanced applications.

## II. EXPERIMENTAL TOOLS AND MATERIALS

**ALD Reactor.** Growth of ZnO and $Al_2O_3$ at various pressures and flow rates was examined using a hot-wall linear flow viscous tubular ALD reactor 60 cm long with 3.8 cm inner diameter, shown schematically in Figure 1.[24] The system exhaust is specially designed to allow two different outlets: one to a vacuum mechanical pump and a second connected directly to the laboratory exhaust vent. The operating pressure is fixed between ∼2 (±10%) and 760 Torr by setting the position of a throttle valve in the vacuum exhaust line and by adjusting the inert $N_2$ gas flow (National Welders, 99.999%).

The inert $N_2$ flows continuously through two gas lines connected directly to the reactor, and the flow rate for each gas line was adjusted using an MKS Unit mass flow controller between 0.25 and 5 standard liters per minute (slm), resulting in a fixed total $N_2$ flow rate between 0.50 and 10 slm. In addition to this fixed $N_2$ flow, a small flow rate (0.50 slm) of $N_2$ was used to "push" the precursor and reactant gas species from their delivery hold cells into the reaction chamber. This additional $N_2$ flow was present only during the reactant and precursor dose times, which was typically 2 s each per ALD cycle. All purge $N_2$ was purified at the gas source using an Aeronex gatekeeper filter (rated to <100 parts per trillion of $H_2O$ and $O_2$).

The gas delivery utilized stainless steel gas hold cells described in more detail below. The pressure in the reactor and in the precursor and reactant hold cells was monitored using convectron pressure gauges (MKS). The reactor temperature was maintained by wrapping the reaction tube exterior walls with heating tape, and the set point was controlled at 100 °C using an Omega temperature controller. The gas hold cells and the delivery lines were likewise controlled at 60 °C. Under sealed conditions, the reactor pump produced a background pressure $<1 \times 10^{-3}$ Torr in the reactor and gas hold cells, and the leak rate was $<1 \times 10^{-3}$ Torr/min.

Diethyl zinc (DEZ, 98% purity, STREM Chemicals) and trimethyl aluminum (TMA, 98% purity, STREM Chemicals) were used as precursors for ZnO and $Al_2O_3$ ALD, respectively, and $H_2O$ (UV-deionized) was used as the reactant. These precursor and reactant reservoirs were maintained at a temperature of 20 °C. Typical cycle times were DEZ/$N_2$/$H_2O$/$N_2$ = 2 s/45 s/2 s/45 s. Growth of ZnO and $Al_2O_3$ by ALD are widely studied, and the processes are well characterized.[25] Under well controlled conditions, TMA/$N_2$/$H_2O$/$N_2$ ALD produces ∼1.1 Å/cycle, or ∼30−40% of an $Al_2O_3$ monolayer.[24−26] Similarly, DEZ/$N_2$/$H_2O$/$N_2$ ALD results in ∼2.0 Å/cycle of ZnO deposition.[27,28] For studies in our reactor in Figure 1, we define "typical conditions" as deposition pressure fixed at 2 Torr, steady-state $N_2$ flow rate of 0.50 slm, and temperature set at 100 °C, and the resulting rates for $Al_2O_3$ and ZnO ALD on oxidized silicon substrates are 1.15 ± 0.1 and 2.0 ± 0.1 Å/cycle, respectively.

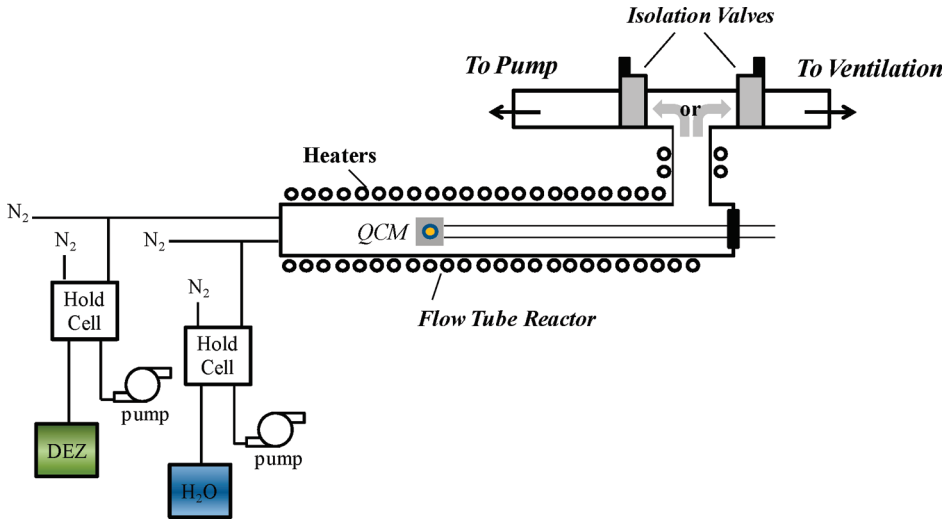


**Figure 1.** Schematic of the modified atomic layer deposition system that offers the ability for materials growth from pressures varying from vacuum to atmospheric conditions in a flow tube reactor design.

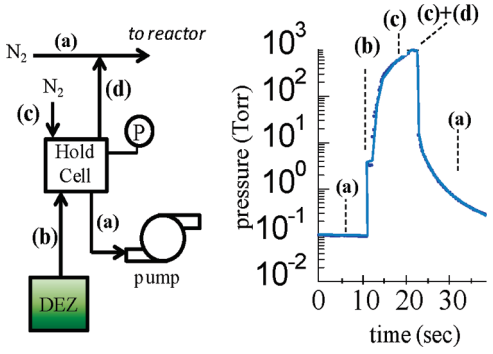


**Figure 2.** Hold cell cycling. Left: schematic of hold cell, precursor source, pump, and pressure gauge. Right: pressure measured in the hold cell as a function of time during the gas delivery cycle. The dashed lines correspond to (a) initial hold cell pump down, achieving a hold cell pressure, $P_{HC} < 10^{-1}$ Torr and $N_2$ purge of reactor; (b) hold cell charge with diethyl zinc to $P_{cell} = P^*_{DEZ}$; (c) hold cell charge with $N_2$ to $P_{cell} >$ 760 Torr; (c) and (d) flow of hold cell contents into the reactor, including continued $N_2$ flow, and (a) $N_2$ purge flow into reactor and pump down of the hold cell to reinitiate cycle.

Under these conditions in our reactor, the Reynolds number is ~2.3 and the Péclet number (discussed below) is <8.5, corresponding to diffusive laminar viscous flow.

**Variable Pressure Precursor Delivery.** To achieve well-defined precursor delivery, a "hold cell" design was developed to allow precursors with low vapor pressure ($P^*$) to be delivered into a reactor operating at higher pressure ($P > P^*$). This delivery scheme serves as a precursor "pressure boost". Separate hold cells are used for each precursor and reactant used. The hold cell gas delivery sequence and the corresponding hold cell pressure measured during one DEZ dose cycle are presented in Figure 2. At the beginning of each cycle, the hold cell is evacuated to $<1 \times 10^{-1}$ Torr by a rotary pump. To begin the gas delivery, the evacuated hold cell is then opened to the source gas for 1 s, allowing reactant vapor to flow in at $P^*$. The convectron gauge shows that the hold cell pressure equilibrates after one second. However, the convectron gauge is not sufficiently accurate in absolute pressure reading to quantify the vapor pressure measurement in this range, so the data in Figure 2 show $P^* <$ 11 Torr. The valve to the precursor is closed, and another valve is opened to higher pressure $N_2$, and the total gas pressure in the cell increases to a predetermined set point, above the desired reactor operating pressure ($P_{cell} \sim > P$). The time needed for this hold cell "charge" depends upon the delivery line conductance, hold cell volume, and the predetermined operating pressure. For the experiments reported here, the DEZ and TMA hold cells were 45 $cm^3$, and they required a charge time of ~11 s to reach $P_{cell}$ ~800 Torr, while the smaller $H_2O$ hold cell (15 $cm^3$) reached 800 Torr in ~6 s. To begin the precursor or reactant exposure, a hold cell outlet valve and a $N_2$ flush inlet line open simultaneously. The $N_2$ flow (0.50 slm) into the hold cell helps flush the precursor or reactant into the reactor for the preset exposure time (typically 2 s). After this exposure step, the cell outlet and flush valves close simultaneously, and the hold cell is opened again to the rotary pump, preparing the system to repeat the cycle. The somewhat elevated pressure in the hold cell relative to the reactor produces a short-term pressure increase which is detected in the reactor pressure gauge and, as discussed below, on the QCM crystal. While this gas flow system allows variable gas delivery pressure, we chose relatively long cycle times for these initial studies. An optimized process could be achieved with significantly shorter cycle times.

Another important parameter of interest in ALD processing is the overall reactant exposure, defined by $L = \int P'(t)\, \partial t$, where $P'$ is the precursor or reactant partial pressure above the growth surface during the dose time. Exposure is often expressed in Langmuir (1 Langmuir, $L = 10^{-6}$ Torr·sec).[1,24] In a typical TMA/$H_2O$ ALD sequence, $10^4$–$10^5$ Langmuir is sufficient to achieve full surface saturation.[24] In a low pressure reactor, where the precursor flows at sonic velocity from a vessel held at the vapor pressure, ($P^*_{TMA} = 11$ Torr)[29] the exposure scales with the dose time, and dose times of less than 1 s are often sufficient to achieve saturation exposure. For the variable pressure reactor described here, the precursor is fed into the reactor for 2 s per cycle, but the net exposure will vary significantly with gas flow and pressure. To understand this we note that the reactor design uses two separately controlled inert gas streams. One stream (fixed here at 0.5 slm) pushes reactant through the hold cell into the reactor, and the other stream (set at values between 0.5 and 5.0 slm) flows directly to the reactor, bypassing the hold cell, and is used to set the reactor gas residence time. If the bypass flow rate is very high, the substrate exposure time is determined by the precursor feed time (i.e., 2 s). However, if the bypass flow rate is low, the gas velocity in the flow tube reactor will be small, so the net gas exposure time can exceed the feed time. This will produce larger precursor exposures at low flow rate, especially at higher pressure.

**Table 1. Values for Exposure, Péclet Number, Residence Time, and Mixing Time Calculated for Different Inert Gas Flow Rates and System Operating Pressures[a]**

| | exposure (Langmuir) | | | Péclet number (@ $v_{max}$) | | |
|---|---|---|---|---|---|---|
| | 2 Torr | 100 Torr | 760 Torr | 2 Torr | 100 Torr | 760 Torr |
| 0.5 slm | $8 \times 10^4$ | $2 \times 10^6$ | $6 \times 10^6$ | 4.2 | 4.2 | 4.2 |
| 1.0 slm | $4 \times 10^4$ | $1 \times 10^6$ | $3 \times 10^6$ | 8.5 | 8.5 | 8.5 |
| 5.0 slm | $8 \times 10^3$ | $2 \times 10^5$ | $6 \times 10^5$ | 42.3 | 42.3 | 42.3 |

| | residence time (sec) | | | mixing time (sec) | | |
|---|---|---|---|---|---|---|
| | 2 Torr | 100 Torr | 760 Torr | 2 Torr | 100 Torr | 760 Torr |
| 0.5 slm | 0.2 | 11 | 82 | $6.1 \times 10^{-3}$ | 0.31 | 2.3 |
| 1.0 slm | 0.1 | 5.5 | 41 | $6.9 \times 10^{-4}$ | $3.5 \times 10^{-2}$ | 0.26 |
| 5.0 slm | 0.02 | 1.1 | 8.2 | $5.4 \times 10^{-6}$ | $2.7 \times 10^{-4}$ | $2.1 \times 10^{-3}$ |

[a] The calculation of exposure is for a 2 s TMA flow time in the gas flow tube reactor with the "pressure boost" delivery design described in the text. Note that the precursor partial pressure, $P'(t)$ is not constant over the TMA flow time, as described in the text. The consumption of the species by the surface area before the sample located at a distance 30 cm from the tube entrance is taken into account, assuming a smooth surface and a completed reaction at every available surface site. The Pe number is provided for the maximum gas velocity. The residence time and mixing times are determined using eqs 2 and 3, respectively.

To estimate the reactant exposure in our reactor, we first evaluate the amount of precursor (in moles) that is delivered into the reactor during the 2 s feed time. We then find the number of moles of inert gas entering during this same time period which then allows us to find the precursor mole fraction in the gas stream. The reactant partial pressure, $P'$, and the time that this gas is exposed to the substrate are then calculated as a function of total pressure and gas flow rate, and $\int P'(t)\,\partial t$ is determined. To estimate the amount of precursor delivered, consider that the hold cell volume, the $N_2$ hold cell flush rate, and hold cell charge pressure are fixed at 45 $cm^3$, 0.5 slm, and 760 Torr, respectively. For TMA with a vapor pressure of 11 Torr, the 45 $cm^3$ hold cell starts with $2.65 \times 10^{-5}$ moles of precursor. With the hold cell parameters fixed, the number of moles of precursor that enters the reactor during the 2 s feed time will depend on the reactor pressure. When the hold cell and reactor are at equal pressure, the hold cell flush rate of 0.5 slm delivers approximately 10% of the hold cell volume to the reactor. Under low reactor pressure operation, the relatively large pressure difference between the hold cell and the reactor will push a larger fraction (taken to be ~50%) of the precursor into the reactor. Using these values, the total exposure was estimated in our reactor geometry for various pressure and flow conditions, and results are shown in Table 1. For example, when the reactor pressure is 2 Torr and the bypass inert gas flow rate is 0.5 slm (i.e., equal to the flow through the hold cell), the volume of gas filled during the 2 s dose moves relatively slowly through the reactor, exposing the substrate to precursor for ~5 s. The net exposure is $\sim 8 \times 10^4$ L, which is sufficient for saturated growth. Increasing the inert gas flow rate to 5.0 slm, at a fixed reactor pressure, increases the gas velocity which in turn decreases the precursor exposure time and the overall dose. Under constant flow conditions, the time the substrate sees the precursor is independent of the system. This is because as pressure is increased under constant flow rate, the dose volume and gas velocity both decrease by the same factor. The decreased volume results in an increase in the dose partial pressure, thereby increasing the overall exposure. These trends follow the values given in Table 1. Note that under the high pressure and high flow rate conditions used here, the estimated TMA precursor exposure is larger than that needed for saturated growth.

**Film Deposition.** Thin films of ZnO and $Al_2O_3$ were deposited on silicon wafers, and film thickness was evaluated using spectroscopic ellipsometry (Alpha SE, J.A. Woollam). The formation of ZnO and $Al_2O_3$ was confirmed by modeling the optical properties of the film using the spectroscopic ellipsometery data from 380 to 900 nm. In situ growth monitoring was conducted using a quartz crystal microbalance (QCM) using an INFICON cool drawer single sensor with the sensor normal perpendicular to the reactant and purge gas flow. The sensor head was modified so the crystal received an inert gas backside purge of ~0.05 slm to maintain good electrical contact of the crystal without ALD film interference. The QCM (INFICON, SC-101, unpolished) operated at a frequency of 6 MHz and the data were recorded at a rate of 7 measurements/second through a Labview CPU interface. To ensure thermal equilibration between the QCM crystal and the system, the crystal was typically allowed to equilibrate in the reactor for several hours before collecting data. Also, to remove effects of previous film growth, 20−25 cycles of fresh deposition were performed on the crystal before data were collected. Several experiments were also performed using cotton fiber mat substrates obtained from Textile Innovators Inc. The fiber mats were woven in a 3 × 1 twill structure and were used as received.

## III. INFLUENCE OF PRESSURE ON ALD REACTOR DESIGN PARAMETERS

The operating pressure of a deposition reactor is determined by the gas flow rate, reactor conductance, and the overall pumping speed. As discussed above, in a typical ALD reactor operating at ~1 Torr, the low pressure allows direct precursor delivery and provides a good balance between convective and diffusive gas transport. Viscous flow is achieved when the Knudsen number, $Kn = \lambda/d$, is <0.01, where $\lambda$ is the mean free path and $d$ is the reactor characteristic dimension (i.e., tube diameter: $d = 3.8$ cm). The gas molecule mean free path is given by $\lambda = 1/(2^{1/2}\pi\alpha^2 n)$ where $\alpha$ is the effective gas molecule diameter (for $N_2$, $\alpha$ ~0.3 nm) and $n$ is the number of molecules per unit volume. Therefore in the flow tube reactor studied here, viscous flow is maintained for all pressures, $P >$ ~0.3 Torr. Direct precursor delivery occurs by precursor gas flowing into the gas feed line at sonic velocity. For diethyl zinc, trimethyl aluminum, and water, $P^*$ is 11, 11, and 17.5 Torr, respectively, at 20 °C.[29,30] For the hold cell design, the precursor delivery is set by the $N_2$ flow rate that flushes the hold cell as well as the pressure drop between the hold cell and the system.

An important parameter for analysis of viscous gas flow is the Reynolds number, Re, defined by the ratio of inertial and viscous forces. This ratio scales as $Re = d\nu\rho/\mu$, where $d$ is the tube diameter, $\nu$ is the gas flow velocity, $\rho$ is the gas density, and $\mu$ is the gas viscosity. At low Re the flow is laminar, and mixing occurs primarily by diffusion. For large Re (typically >2100), turbulence becomes important and mixing occurs more readily. For typical ALD operating conditions at 2 Torr and total flow rate of 0.50 slm, using the viscosity of $N_2$ $\sim 0.22 \times 10^{-4}$ g/cm·s at 100 °C, the Re value is ~11.6. This value is independent of pressure at fixed flow rate because the higher pressure (i.e., increased density) is balanced by decreased gas velocity. Viscosity also is independent of pressure, but it does increase with temperature ($\mu \propto T^{1/2}$) so that increasing temperature will tend to reduce the Reynolds number.[31] Increasing the $N_2$ flow rate to 10 slm will increase Re to 232 at 100 °C, still well within the laminar flow regime.

In ALD processing we are concerned with the rate at which physisorbed reactants or vapor products formed during the surface growth reaction will diffuse away from the surface and be removed by

the purge gas flow. The system Péclet number is determined by the ratio of species transport due to convective flow to that due to diffusive flow[32] and will therefore give insight into diffusive species interaction with convective flow. The Péclet number is given as Pe = $dv/D_{12}$ where $d$ is the tube diameter, $v$ is gas velocity, and $D_{12}$ is the diffusion coefficient for the product (species 1) into the inert gas stream (species 2). At low Péclet number, diffusive transport dominates, and species are readily removed from the surface and become entrained into the purge gas flow. Species diffusivity decreases linearly with pressure as $1/P$, and in laminar flow the gas velocity changes with radial position, so the Péclet number will depend on flow rate and radial position in the reactor. Under constant mass flow conditions, the Péclet number remains constant when pressure changes. While diffusivity depends on temperature, the effect of pressure on diffusivity is more pronounced. An estimate of the diffusion coefficient, $D_{12}$, for reactant species in the carrier gas, $N_2$, can be determined by the diffusion of $CH_4$ in $N_2$.[31,33] For a processing temperature of 100 °C, $D_{12}$ is 125 and 0.33 $cm^2/s$ at 2 and 760 Torr, respectively. Therefore, the Péclet number under typical ALD flow conditions (2 Torr, 0.50 slm) is very small near the tube wall and increases to Pe = 4.2 where the gas velocity is largest ($v_{max}$) at the tube center. The process is sufficiently diffusive to enable rapid transport of surface products out of the reactor. When the pressure and flow rate increase to 760 Torr and 5.0 slm, respectively, the Péclet number stays small near the wall, but it increases rapidly to Pe = 42 near the tube center, indicating that gas transport will rely more on convection under the high pressure/high flow conditions. The Péclet numbers calculated at $v_{max}$ for various values of gas flow rate and pressure are provided in Table 1.

The effect of process pressure on gas transport can also be evaluated by considering the mean displacement distance of a diffusing species:

$$x = \sqrt{6D_{12}t} \quad (1)$$

where the factor of 6 corresponds to diffusion in three dimensions, and $t$ is the time the species is allowed to diffuse with diffusion coefficient $D_{12}$. For the $D_{12}$ values above, the mean displacement distance during 1 s is ~27.4 cm at 2 Torr, and ~1.4 cm at 760 Torr. This again highlights the fact that diffusive transport becomes less dominant as reaction pressure increases to atmospheric pressure.

The purge time needed in the ALD sequence to ensure negligible reactant/precursor interaction is often determined using the average gas residence time, $\tau$, as a lower bound. The gas residence time is defined by

$$\tau = \frac{PV}{Q_T} \quad (2)$$

where $P$ is the operating pressure, $V$ is in the reactor volume, and $Q_T$ is the gas throughput (typically given in Torr liters per second). For the flow tube reactor used here, the calculated gas residence time is shown in Table 1 as a function of pressure and total gas flow rate.

Figure 3 shows a plot of gas residence time in our reactor as a function of pressure for two values of gas flow rate. At 760 Torr and 0.50 slm the long gas residence time ($\tau$ = 82 s) could lead to interaction between the precursor and reactant, producing chemical vapor deposition and a larger than expected growth rate if the purge time is too short. The expected transition from

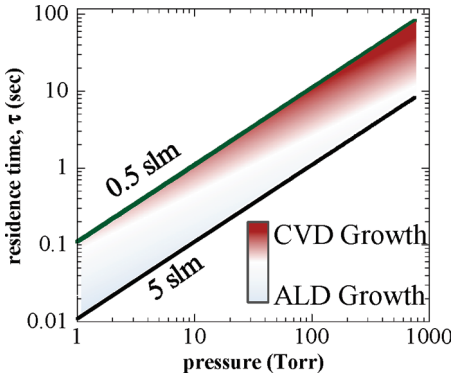


**Figure 3.** Plot of residence time ($\tau = PV/Q$) determined as a function of flow tube operating pressure. The gradient mapping shows the regions for anticipated CVD-type and ALD-type growth. The residence time is calculated as the time for a pulse of gas from the hold cell to move through a flow tube with length of 60 cm diameter of 3.8 cm. The flow rate represents that of the purge gas.

ALD to CVD conditions is shown schematically by the shading in Figure 3, where the darker area corresponds to regions where CVD conditions are expected, and lighter shading corresponds to more ALD growth for the typical gas purge times used in this work. A longer purge time will result in an increase in the ALD growth region. However, shorter gas purge times and residence times are desired in ALD in order to increase process throughput.

In addition to the gas residence time, another important parameter in the process and reactor design is the time needed for physisorbed reactive species (such as water) or vapor product species generated during the growth reactions on the surface to diffuse away from the growth surface and become mixed into the convective gas flow. By considering the diffusion velocity and the Péclet number, we estimate a relative gas "mixing time" needed for a species diffusing off the flow tube wall to be collected into the convective flow stream. This relative mixing time, $t_m$, is obtained by integrating the diffusive velocity ($v_D = 3D_{12}/r$) as a function of radial position from the tube wall (where convective velocity and Pe are small) to the point ($r'$) where the Pe = 1 (i.e., where species transport by convection is equivalent to that by diffusion):

$$t_m = \int_0^{r'} \frac{1}{v_D(r)}\, dr \quad (3)$$

The calculated values for the mixing time as a function of gas flow rate and pressure are also given in Table 1. For a system operating with a gas flow rate of 0.50 slm, the mixing time is on the order of $6.1 \times 10^{-3}$ s at 2 Torr and increases in proportion with pressure to 2.3 s at 760 Torr. Increases in the gas flow rate decreases the mixing time.

The continuum flow analysis indicates that at 760 Torr, the 45 s purge time and 5.0 slm flow rate are sufficient to maintain the gas residence time and mixing time within the regime expected for good quality ALD. We note that at a fixed temperature, the rate of water desorption will depend upon specific physisorption energies and desorption barriers that depend on the specific oxide studied. These continuum gas flow calculations do not attempt to model the specific species desorption kinetics, but they do present general guidelines to analyze ALD reactor design parameters. We next consider experimental results of growth rate versus pressure and gas flow.

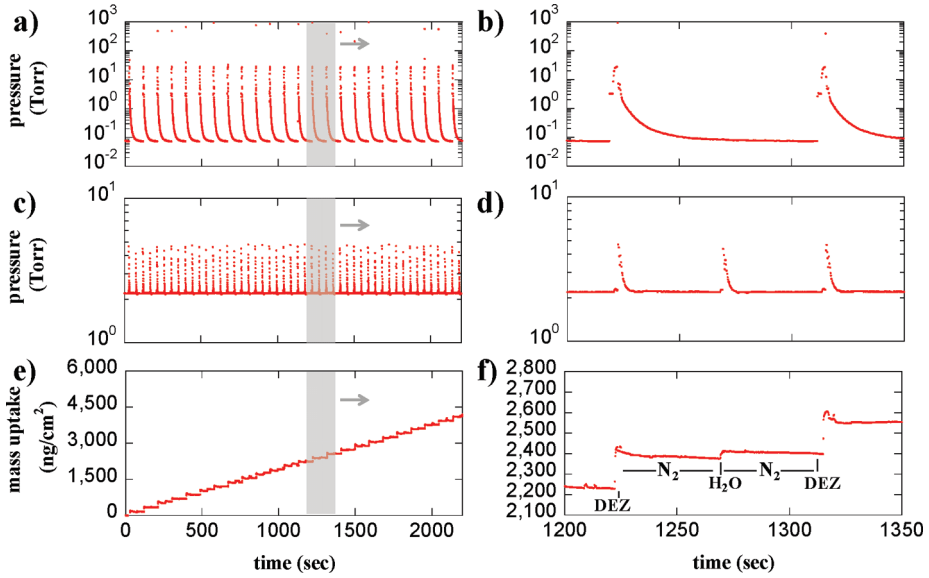


**Figure 4.** Pressure recording of the (a,b) diethylzinc (DEZ) hold cell and (c,d) flow tube deposition, as well as the (e,f) corresponding quartz crystal microbalance mass uptake data for consecutive DEZ/$N_2$/$H_2O$/$N_2$ cycles at a pressure of 2 Torr. The DEZ hold cell pressure, system pressure, and mass uptake for the 14th and 15th ZnO deposition cycle are shown on the figures to the right. The data were recorded with a purge gas flow rate of ~0.50 slm and a process temperature of 100 °C.

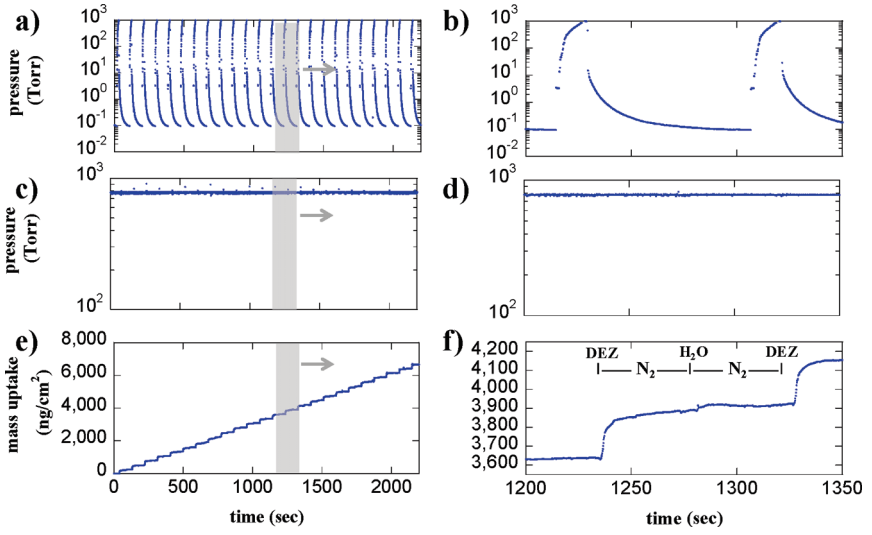


**Figure 5.** Pressure recording of the (a,b) diethylzinc (DEZ) hold cell and (c,d) flow tube deposition, as well as the (e,f) corresponding quartz crystal microbalance mass uptake data for consecutive DEZ/$N_2$/$H_2O$/$N_2$ cycles at a pressure of 760 Torr. The DEZ hold cell pressure, system pressure, and mass uptake for the 14th and 15th ZnO deposition cycle are shown on the figures to the right. The data were recorded with a purge gas flow rate of ~0.50 slm, and a process temperature of 100 °C.

## IV. RESULTS AND DISCUSSION

**Quartz Crystal Microbalance Analysis of ZnO Deposition vs Pressure and Flow Rate.** Real-time pressure and quartz crystal microbalance results collected during ZnO growth in our reactor at 2 Torr are provided in Figure 4. The operating temperature was 100 °C and the inert gas flow rate was 0.50 slm. Pressure monitoring of the DEZ hold cell pressure over 25 cycles (Figure 4a), shows consistent behavior of the precursor pressure boost sequence in the hold cell. Closer detail of the hold cell pressure of the 14th and 15th cycles (Figure 4b) shows the inert gas charge pressure was 40 Torr, which is well above the 2 Torr operating pressure. Figure 4c and d show the reactor pressure as a function of time during the DEZ and $H_2O$ exposure cycles. The gas delivery sequence results in a momentary increase in system pressure, returning to the 2 Torr set point after a few seconds. Figure 4e and f show data from the in situ quartz crystal microbalance placed in the reactor 30 cm downstream from the gas inlet. The mass increase is linear over 25 cycles (Figure 4e), and mass uptake during one example cycle (Figure 4f) shows a net increase of ~150 and 20 ng/cm$^2$ during the DEZ and $H_2O$ pulses, respectively, consistent with prior results of ZnO ALD growth on similar unpolished QCM crystals.[27] The initial spike and decrease in mass gain upon gas exposure are associated with the pressure transients shown in Figure 4d. Control experiments (discussed below) show that the instantaneous pressure increase does not contribute to the overall mass increase on the QCM surface.

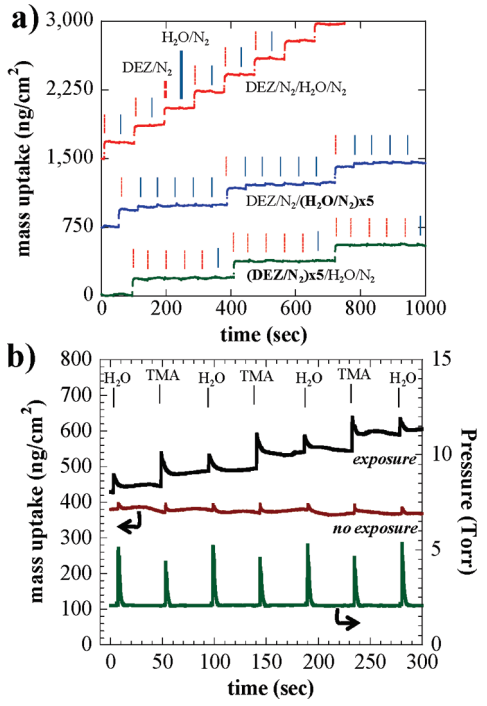


**Figure 6.** (a) Saturation measurements at a system operating pressure of 760 Torr examined by mass uptake data. In the plot, sequential DEZ/$N_2$/$H_2O$/$N_2$ cycles are compared to a single DEZ/$N_2$ exposure followed by 5 consecutive $H_2O$/$N_2$ exposures and a single $H_2O$/$N_2$ exposure followed by 5 consecutive DEZ/$N_2$ exposures. The data were recorded at a purge gas flow rate of 0.50 slm and a process temperature of 100 °C. (b) Plot of mass uptake for consecutive TMA/$N_2$/$H_2O$/$N_2$ cycles with and without a TMA and water hold cell charge steps. The corresponding pressure in the system is provided on the secondary axis. The $N_2$ hold cell charge pressure was ~40 Torr.

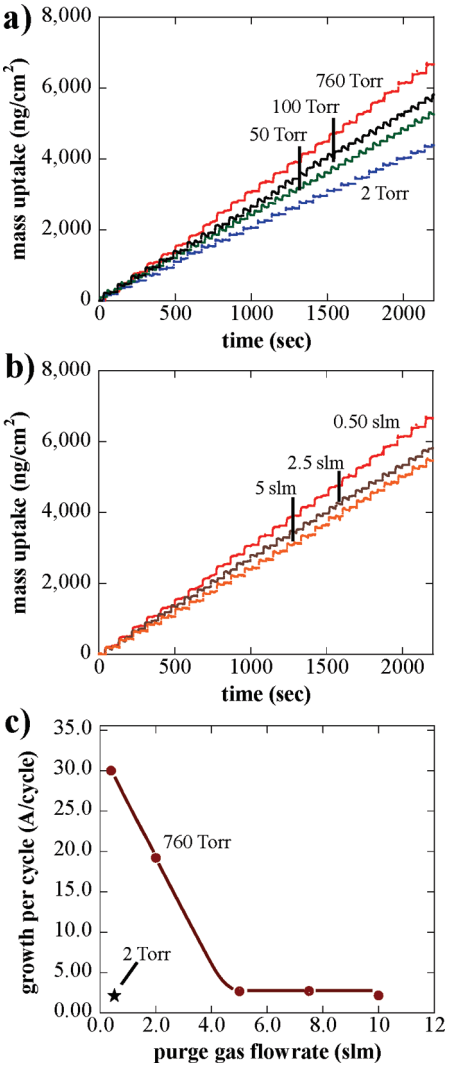


**Figure 7.** (a) Mass uptake data for consecutive DEZ/$N_2$/$H_2O$/$N_2$ cycles at a system operating pressure of ~2, 50, 100, and 760 Torr with a purge gas flow rate of 0.50 slm and a process temperature of 100 °C. (b) Similar data collected at 760 Torr and an $N_2$ flow rate of 0.50, 2.50, and 5.0 slm. (c) Average growth per cycle of ZnO at 760 and 2 Torr using 30 s purge times plotted against purge gas flow rate. At 5.0 slm the growth rate at 760 Torr is the same as at 2 Torr.

Figure 5 shows similar pressure and QCM results obtained during ZnO growth at 760 Torr with flow rate fixed at 0.50 slm and $T$ = 100 °C. Figure 5a and b show the hold cell pressure oscillation between 0.07 and ~800 Torr during the reaction cycle. In Figure 5b, the pressure first increases when DEZ fills the hold cell to $P^*_{DEZ}$, then it increases further when the hold cell is charged with $N_2$ to the final pressure. The pressure in the reactor (Figure 5c and d) remains constant at 760 Torr, although some low magnitude pressure transients may appear during the gas dosing steps. Similar to the results at 2 Torr, the QCM data (Figure 5e and f) shows linear mass uptake over 25 cycles, but the mass uptake is ~250 and 20 ng/cycle during the $H_2O$ and DEZ steps, respectively, which is significantly larger than at 2 Torr and consistent with excess CVD growth.

As a control experiment, the QCM crystal was exposed to repeated DEZ/$N_2$ cycles without the water exposure step. As shown in Figure 6a, after the first exposure cycle, no mass uptake was observed for subsequent DEZ exposures, consistent with negligible water contamination in the reactor system. Similarly, repeated $H_2O$/$N_2$ exposures after one DEZ/$H_2$ step showed negligible mass uptake after the first dose. Another control experiment was used to explore the effect of pressure on the QCM response, and the results are shown in Figure 6b. We examined the QCM at $P$ = 2 Torr and 0.50 slm $N_2$ flow, using a $N_2$ hold cell charge of 760 Torr. The data show pressure measured in the hold cell, as well as the QCM signal plotted during gas exposure cycles. The pressure spike corresponds to the $N_2$ charge gas flowing into the chamber from the hold cell, and the magnitude of the pressure spike is determined by the hold cell charge pressure. The lower QCM trace shows results when the valves between each gas source and hold cell were closed, resulting in no net growth. Data collected when they were open, producing a net mass uptake, are also shown. This data set was collected during $Al_2O_3$ growth using TMA and water cycles. With the gas valves closed, transient spikes are observed in the QCM corresponding to the pressure increase, with no net mass change. Under deposition conditions, the spikes in the QCM data are somewhat larger than for pressure change only, suggesting the QCM response corresponds to both pressure and precursor adsorption/desorption effects.

Figure 7a shows QCM results during DEZ/$H_2O$ cycles for different gas pressures between 2 and 760 Torr using 0.50 slm $N_2$ and $T$ = 100 °C. At each deposition pressure, the hold cell was charged with $N_2$ to ~800 Torr. The mass uptake per cycle is larger at higher deposition pressure. This is consistent with CVD

growth resulting from the long gas residence time at high pressure, as shown in Figure 3. Data in Figure 7b show that at 760 Torr, increasing the flow from 0.50 to 5.0 slm produces a decrease in the mass uptake, consistent with transition away from CVD at short gas residence time. The growth per cycle average over 100 ALD cycles is shown in Figure 7c versus pressure using 0.50 slm $N_2$ and purge time of 30 s. This indicates that $N_2$ flow >5.0 slm (i.e., $\tau \leq 8$ s) is needed to achieve ~2.0 A/cycle at 760 Torr in our reactor.

**Comparison of ZnO and $Al_2O_3$ ALD at Atmospheric Pressure.** We also explored ALD $Al_2O_3$ at various pressures and flow rates, and trends similar to that shown for DEZ/$H_2O$ were observed. We are interested to find if the different metal oxides show any differences in growth under AP-ALD conditions. Figure 8a and b show QCM data collected during ZnO and $Al_2O_3$ deposition, respectively, at low pressure/low flow rate (2 Torr/0.50 slm) and at high pressure/high flow rate (760 Torr/5.0 slm). These conditions were chosen to approach reasonably good ALD growth at both low and high pressure (as shown schematically in Figure 3). In these experiments, the hold cell was charged to 40 Torr and ~800 Torr for reactor pressures of 2 and 760 Torr, respectively. For the DEZ/$H_2O$ process, the results in Figure 8a show a transient increase in the QCM signal at the start of each pulse, consistent with pressure spikes. The average mass uptake during the DEZ dose is ~175 ± 20 ng/cm at 760 Torr and 5.0 slm, which is reasonably similar to ~145 ± 15 ng/cm obtained at 2 Torr and 0.50 slm. For the TMA/$H_2O$ results shown in Figure 8b, spikes in the QCM data are also observed. The mass uptake scale is more magnified for the TMA/$H_2O$ process, and therefore, the effects due to pressure transients appear to be more pronounced. The average mass uptake during the TMA dose is ~66 ± 15 ng/cm at 760 Torr and 5.0 slm, which is nearly a factor of 2 larger than the value of ~37 ± 15 ng/cm obtained at 2 Torr and 0.50 slm. This change in growth rate at higher pressure in the TMA/$H_2O$ process compared to minimal change in the DEZ/$H_2O$ process suggests interesting differences in the ZnO and $Al_2O_3$ ALD mechanisms.

There are several plausible reasons to explain the excess growth rate for $Al_2O_3$ observed under high pressure conditions. One possibility is that the very large exposures used here produce a surface saturation that is larger than that typically observed at low pressure. Wind et al.[34] recently showed that during $Al_2O_3$ ALD, an increase in the TMA and water exposures to values larger than that typically needed for saturation under typical conditions resulted in a growth rate increase of ~25−30%. As shown above, the TMA and water exposure used here are significantly larger than those under typical low pressure deposition conditions. This increased exposure may result in a change in the adsorption and desorption kinetics of the precursor and reactant on the sample surface, and slow water desorption may result in a CVD component to film growth. Other results not shown also suggest that the ALD "temperature window" will depend on deposition pressure. Adsorbed water may also promote excess TMA adsorption, for example, if the TMA remains in the dimer state when impinging on the surface. The gas flow model discussed above shows that the flow conditions are sufficient to achieve good entrainment of diffusing species during the purge, so more detailed kinetic models that take into account species surface desorption rates will provide further insight.

**Application of AP-ALD to High Surface Area Textile Substrates.** We are interested in applying AP-ALD to high surface area substrates of complex surface structure such as nonwoven

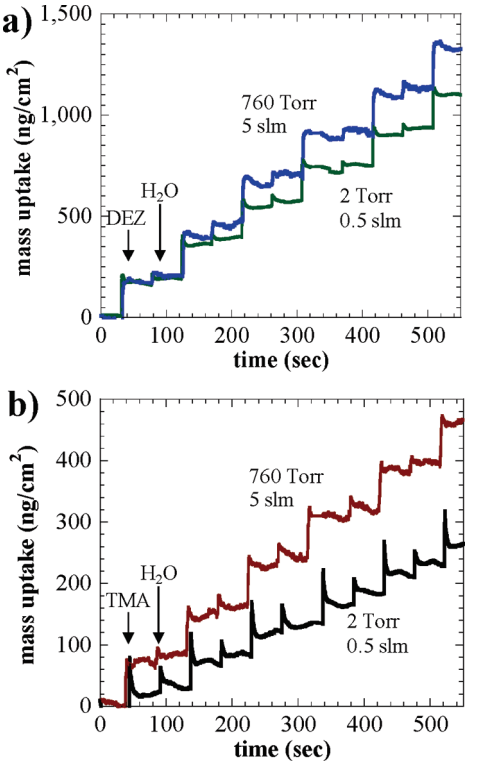


**Figure 8.** Plot of (a) ZnO mass uptake at 760 Torr, 5.0 slm and 2 Torr, 0.50 slm growth; (b) comparable plots for $Al_2O_3$ growth at 760 and 2 Torr. Data were recorded at a process temperature of 100 °C.

fiber media, textiles, and other porous structures. Reports to date for high pressure ALD have focused primarily on planar substrates. Porous substrates present a tortuous flow pathway that the ALD precursor and reactant must infiltrate, and the flow tube reactor geometry presented here provides a means to coat these materials at high pressure. Coating processed woven cotton fabrics with a few cycles of $Al_2O_3$ ALD can result in a dramatic change in the wetting properties of the material from hydrophilic to hydrophobic.[6] With a thicker coating, the surface reverts back to hydrophilic. Therefore, monitoring the wetting properties of cotton after AP-ALD treatment provides a test for the presence of a consistent modified surface with a conformal nanoscale thickness. For this experiment, a hydrophilic (fully wetting, water contact angle ~0°) ~1.5 × 1.5 cm$^2$ woven cotton sample was oriented in the AP-ALD flow reactor in a "flow through" geometry, i.e., with its surface oriented normal to the gas flow direction, and it was exposed to 2 ALD cycles (TMA/$N_2$/$H_2O$/$N_2$ = 2/45/2/45 s) at 100 °C using an inert gas flow rate of 5.0 slm at 760 Torr. The results of wettability tests after deposition are shown in Figure 9. The cotton mat shows hydrophobic character, with a water contact angle >115° on both the front and back of the material (bottom images in Figure 9), consistent with a uniform and conformal thin coating on the sample fibers. The conformality of the coating on the cotton samples prepared here was not directly characterized. However, the wetting results obtained are consistent with those reported in reference 6 where conformal coverage was directly characterized by transmission electron microscopy. In comparison, a cotton mat treated with 2 cycles $Al_2O_3$ at 0.50 slm at 760 Torr (outside the expected ALD range) shows a contact angle <90° on the front and rear, consistent with a thicker coating. A thicker coating is expected under

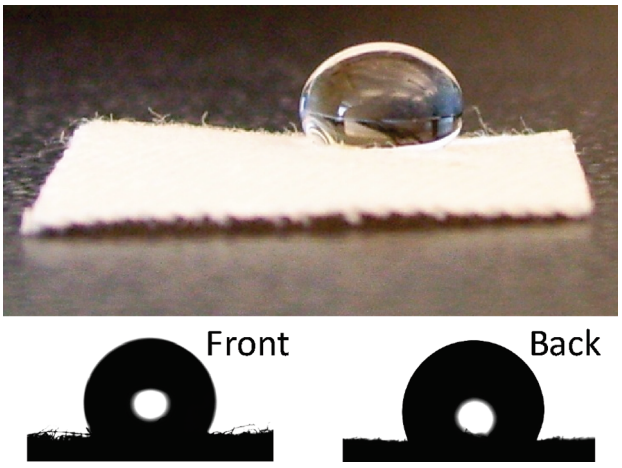


**Figure 9.** Image of water droplet on a cotton fabric that has been modified by 2 cycles of $TMA/N_2/H_2O/N_2$. The images below show a contact angle >115° on both the front and back of the cotton fabric indicating that the entire cotton fabric was coated.

these conditions, as presented above and in Figure 7 for the growth rate analysis on planar substrates. For this porous sample, we can also estimate the overall surface area and therefore determine the minimum TMA and water dose required in each ALD cycle to achieve near monolayer coverage. Brunauer−Emmett−Teller (BET) analysis shows the uncoated woven cotton has a surface area of ∼1 $m^2/g$ (which is expected to stay approximately constant upon coating). A woven cotton sample of 40 $cm^2$ has a mass of 1 g, so the surface area enhancement factor (net surface area/projected surface area) is ∼250×. We estimate the minimum amount of precursor needed to coat this surface by assuming that all TMA that flows into the fiber mat reacts with available reactive sites. This is reasonable even for nonunity sticking coefficient considering the tortuous pathway for precursor transport through the substrate. For a TMA hold cell volume of 45 $cm^3$, the amount of precursor delivered at high pressure and high flow rate is sufficient to conformally coat the smooth reactor wall and a sample >5 $cm^2$ in size (i.e., total surface area >1250 $cm^2$), which is much larger than the ∼2.5 $cm^2$ sample size used in this experiment. These results therefore show initial feasibility of atmospheric pressure ALD of $Al_2O_3$ and ZnO, including application to through-porous substrates including woven fibrous materials.

## V. CONCLUSIONS

This work describes an atomic layer deposition system compatible with processing between 2 Torr and atmospheric conditions. A novel "pressure boost" delivery scheme was integrated into a flow tube reactor allowing high pressure precursor delivery. Mass uptake measured during ALD cycling shows the transition from CVD at high pressure and low gas flow rates, toward ALD at higher flow rates at higher pressure, consistent with ALD conditions under shorter gas residence times. We showed that other parameters, including Reynolds number, Péclet number, and mixing time are also important to obtain well controlled ALD, and the relations among these values and pressure and flow rate were analyzed in a continuum flow model. We conclude that in our reactor system, a $N_2$ flow rate of 5.0 slm is sufficient at 760 Torr to achieve highly diffusive gas transport, where surface products readily entrain into the convective gas flow stream during the purge cycle time. Under these conditions, however, we observe a higher growth rate than expected for TMA/water ALD, whereas the DEZ/water process results in rates very similar to a typical 2 Torr, 0.50 slm ALD process. The excess mass uptake during $Al_2O_3$ deposition is ascribed to surface species adsorption/desorption kinetic effects. For example, a higher enthalpy for water desorption from Al−OH--$H_2O$ versus Zn−OH--$H_2O$ will leave excess water on the alumina surface, producing a higher than expected growth rate. High surface area cotton textile materials coated using the AP-ALD reactor system show the same transitions in wetting properties as similar materials coated using more conventional ALD conditions, consistent with conformal and well controlled ALD at atmospheric pressure. Insights gained here will help understanding of new high throughput ALD processes, for example, using roll-to-roll platforms.

## AUTHOR INFORMATION

**Corresponding Author**
*E-mail: jsjur@ncsu.edu.

## ACKNOWLEDGMENT

This research was financed by the United States National Science Foundation CMMI: Nanomanufacturing Grant No. 1000382.

## REFERENCES

(1) George, S. M. *Chem. Rev. (Washington, DC, U. S.)* **2010**, *110*, 111–131.
(2) Kim, H. *J. Vac. Sci. Technol., B* **2003**, *21*, 2231–2261.
(3) Leskela, M.; Ritala, M. *Angew. Chem., Int. Ed.* **2003**, *42*, 5548–5554.
(4) Peng, Q.; Gong, B.; VanGundy, R. M.; Parsons, G. N. *Chem. Mater.* **2009**, *21*, 820–830.
(5) Na, J. S.; Ayres, J. A.; Chandra, K. L.; Gorman, C. B.; Parsons, G. N. *J. Phys. Chem. C* **2008**, *112*, 20510–20517.
(6) Hyde, G. K.; Scarel, G.; Spagnola, J. C.; Peng, Q.; Lee, K.; Gong, B.; Roberts, K. G.; Roth, K. M.; Hanson, C. A.; Devine, C. K.; Stewart, S. M.; Hojo, D.; Na, J. S.; Jur, J. S.; Parsons, G. N. *Langmuir* **2009**, *26*, 2550–2558.
(7) Jur, J. S.; Spagnola, J. C.; Lee, K.; Gong, B.; Peng, Q.; Parsons, G. N. *Langmuir* **2010**, *26*, 8239–8244.
(8) Charton, C.; Schiller, N.; Fahland, M.; Hollander, A.; Wedel, A.; Noller, K. *Thin Solid Films* **2006**, *502*, 99–103.
(9) Hoppe, H.; Sariciftci, N. S. *J. Mater. Res.* **2004**, *19*, 1924–1945.
(10) Mayer, A. C.; Scully, S. R.; Hardin, B. E.; Rowell, M. W.; McGehee, M. D. *Mater. Today* **2007**, *10*, 28–33.
(11) Mahltig, B.; Haufe, H.; Bottcher, H. *J. Mater. Chem.* **2005**, *15*, 4385–4398.
(12) *Handbook of Nonwovens*; Russell, S. J., Ed.; Woodhead: Cambridge, U.K., 2007.
(13) Suntola, T. S.; Pakkala, A. J.; Lindfors, S. G. U.S. Patent 4,389,973, 1983.
(14) Dapkus, P. D.; Maa, B. Y.; Chen, Q.; Jeong, W. G.; Denbaars, S. P. *J. Cryst. Growth* **1991**, *107*, 73–82.
(15) Dunlop, L.; Kursumovic, A.; MacManus-Driscoll, J. L. *Appl. Phys. Lett.* **2008**, *93*, No. 172111.
(16) Hunter, A.; Kitai, A. H. *J. Cryst. Growth* **1988**, *91*, 111–118.
(17) Kaiya, K.; Yoshii, N.; Omichi, K.; Takahashi, N.; Nakamura, T.; Okamoto, S.; Yamamoto, H. *Chem. Mater.* **2001**, *13*, 1952–1956.
(18) Kaiya, K.; Yoshii, N.; Takahashi, N.; Nakamura, T. *J. Mater. Sci. Lett.* **2000**, *19*, 2089–2090.
(19) Levy, D. H.; Freeman, D.; Nelson, S. F.; Cowdery-Corvan, P. J.; Irving, L. M. *Appl. Phys. Lett.* **2008**, *92*, No. 192101.

(20) Nonobe, S.; Takahashi, N.; Nakamura, T. *Solid State Sci.* **2004**, *6*, 1217–1219.
(21) Takahashi, N.; Nonobe, S.; Nakamura, T. *J. Solid State Chem.* **2004**, *177*, 3944–3948.
(22) Takahashi, N.; Yoshii, N.; Nonobe, S.; Nakamura, T.; Yoshioka, M. *J. Electron. Mater.* **2003**, *32*, 1107–1110.
(23) Yoshii, N.; Takahashi, N.; Nakamura, T.; Yoshioka, M. *Electrochem. Solid-State Lett.* **2002**, *5*, C85–C86.
(24) Elam, J. W.; Groner, M. D.; George, S. M. *Rev. Sci. Instrum.* **2002**, *73*, 2981–2987.
(25) Puurunen, R. L. *J. Appl. Phys.* **2005**, *97*, No. 121301.
(26) Puurunen, R. L. *Appl. Surf. Sci.* **2005**, *245*, 6–10.
(27) Na, J. S.; Peng, Q.; Scarel, G.; Parsons, G. N. *Chem. Mater.* **2009**, *21*, 5585–5593.
(28) Schuisky, M.; Elam, J. W.; George, S. M. *Appl. Phys. Lett.* **2002**, *81*, 180–182.
(29) Bamford, C. H.; Levi, D. L.; Newitt, D. M. *J. Chem. Soc.* **1946**, 468–471.
(30) Wagner, W.; Pruss, A. *J. Phys. Chem. Ref. Data* **2002**, *31*, 387–535.
(31) Hirschfelder, J. O.; Bird, R. B.; Spotz, E. L. *Chem. Rev. (Washington, DC, U. S.)* **1949**, *44*, 205–231.
(32) Leal, L. G. *Laminar Flow and Convective Trasnport Processes*, 1st ed.; Butterworth-Heinemann: Newton, MA, 1992.
(33) Geankoplis, C. *Tansport Processes and Unit Operations*, 3rd ed.; Prentice Hall: Englewood Cliffs, NJ, 1993.
(34) Wind, R. A.; George, S. M. *J. Phys. Chem. A* **2010**, *114*, 1281–1289.